



## RESEARCH ARTICLE

## Oxidative Chemical Polymerization, Kinetic Study, Characterization and DFT Calculations of Para-Toluidine in Acid Medium Using $K_2Cr_2O_7$ as Oxidizing Agent

S. M. Sayyah<sup>1\*</sup>, H.M.Mustafa<sup>2</sup>, A.H. El-Ghandour<sup>1</sup>, A.A.Aboud<sup>3</sup> and M.Y. Ali<sup>1</sup>

1. Chemistry Department, Faculty of Science, BeniSuef University 62514 Beni-Suef, Egypt.

2. Chemistry Department, Faculty of Science, Cairo University.

3. Physics Department, Faculty of Science, BeniSuef University 62514 Beni-Suef, Egypt

### Manuscript Info

#### Manuscript History:

Received: 12 February 2015  
Final Accepted: 22 March 2015  
Published Online: April 2015

#### Key words:

oxidative chemical polymerization,  
p-toluidine characterization,  
kinetics, electrical conductivity

#### \*Corresponding Author

S. M. Sayyah

### Abstract

The synthesis of poly-p-toluidine (PpTO) by oxidative chemical polymerization using potassium dichromate as oxidizing agent was carried out. The optimum conditions for the polymerization reaction were investigated. The order of reactions and thermodynamic activation parameters were calculated. A molecular mechanism for the oxidation of p-toluidine using potassium dichromate is proposed. This mechanism explains the specific features of p-toluidine oligomerization and polymerization reactions. Spectroscopic studies using IR, UV-vis and elemental analysis have evidenced the structure of polymeric chain. The surface morphology of the obtained polymer was characterized by X-ray diffraction and transmission electron microscopy (TEM). The thermo gravimetric analysis (TGA) was used to confirm the proposed structure and number of water molecules in each polymeric chain unit. Moreover, determinations of dielectric properties of the prepared polymer were carried out. The a.c conductivity ( $\sigma_{ac}$ ) of (PpTO) was investigated as a function of frequency and temperature. The microscopic conduction mechanism of charge carries over the potential barrier in polymer backbone was found classical hopping model.

Copy Right, IJAR, 2015., All rights reserved

## INTRODUCTION

Conducting polymers have been extensively studied due to their interesting electrical and electrochemical properties[1]. The ability of conjugated polymers to carry delocalized electronic charges is used in many applications in which metallic, semi-conducting or electrically tunable medium is involved [2,3,4]. Polyaniline is a typical phenylene based polymer having a chemically flexible –NH– group in a polymer chain flanked either side by a phenylene ring. It can also be defined as the simple 1, 4- coupling product of monomeric aniline molecule. The protonation and deprotonation and various other physico-chemical properties of polyaniline is due to the presence of the –NH– group. Polyaniline (PANI) and polyaniline derivatives are the most extensively studied electro-conductive polymers and they are important members in the intrinsically conductive polymers (ICP) family. Polyaniline is ease of preparation, excellent environmental stability, various forms, interchangeable oxidation states, electrical, optical properties and economic cost[5,6,7].

The aniline derivatives which prepared chemically are almost all donating substitution on benzene ring as (alkyloxy, hydroxy, chloroaniline, etc..) and also at the nitrogen atom was reported by S.M.Sayyah et al [8,9,10,11] to improve the solubility of polyaniline. The kinetics of chemical polymerization of 3-methylaniline, 3-chloroaniline, 3-hydroxyaniline, 3-methoxyaniline and N-methyl aniline in hydrochloric acid solution using

potassium dichromate as oxidant and characterization of the polymer obtained by IR, UV-visible and elemental analysis, X-ray diffraction, scanning electron microscopy, TGA-DTA analysis and a.c conductivity have been reported by S.M.Sayyah et al [12,13,14].

In the absence of any systematic study of the electronic properties and bonding characterization of these classes of polymer, most conclusions that relate the activities to structural factors are qualitative. The main objectives of the present work are to:

- 1- Study the kinetics of the oxidative chemical polymerization using potassium dichromate as oxidant for p-toluidine monomer in aqueous HCl medium.
- 2- Investigate closely the ground state electronic structure and stability of p-toluidine radical cation.
- 3- Theoretically explore the step by step formation of polymeric chain.
- 4- The obtained polymer is characterized by IR, UV-visible, TGA, elemental analysis, X-ray, transmission electron microscopy (TEM) and a.c conductivity measurements.

## Experimental

### 2.1. Materials:

P-toluidine provided by Honeywell Chemical Co., (Germany). Concentrated hydrochloric acid, pure grade product, provided by El-Nasr pharmaceutical chemical Co., Egypt. Potassium dichromate provided by Sigma-Aldrich chemical Co., (Germany). Doubly distilled water was used to prepare all the solutions needed in the kinetic studies.

### 2. 2. Oxidative Aqueous Polymerization of p-Toluidine Monomer:

The polymerization reaction was carried out in a well-stoppered conical flask of 100 ml capacity; addition of p-Toluidinemonomer (pTO) amount in 15ml HCl of known molarity followed by addition of the required amount of potassium dichromate as oxidant in water (10 ml) to the reaction mixture. The orders of addition of substances were kept constant in all the performed experiments. The stoppered conical flasks were then placed in an automatically controlled thermostat at the required temperature. The flasks were shaken (15 shakings/ 10s /30 min) by using an automatic shaker. The flasks were filtrated using a Buchner funnel, and then the obtained polymer was washed with distilled water, and finally dried till constant weight in vacuum oven at 60°C.

### 2.3. Calculations:

#### 2.3.1. Determination of Conversion Yield:

The conversion yield of the monomer to the polymer was determined by the weighing of the dry obtained polymer (P) divided by the weight of the monomer (w) and was calculated in the following way:

$$\text{Conversion yield \%} = \frac{\text{Polymer Yield}(P)}{\text{Weight of Momoner}(w)} \times 100 \quad (1)$$

#### 2.3.2. Determination of the Polymerization Rate:

The rate of polymerization was determined by the following equation:

$$\text{Rate}(R_i) = \frac{P}{V \times M. wt \times t} \text{ (gmol/L. sec)} \quad (2)$$

Where (P) is the weight of polymer formed at time (t) in seconds, (V) is the volume of the reaction solution in liters and (M.wt) is the molecular weight of the monomer[15].

#### 2.3.3. Calculation of the Apparent Energy of Activation.

The apparent activation energy ( $E_a$ ) of the aqueous polymerization reaction was calculated using the following Arrhenius equation:

$$\text{Log}(K) = \frac{-E_a}{2.303RT} + C \quad (3)$$

where (K) is the rate, (R) is the universal gas constant, T is the reaction temperature and (C) is constant [16].

#### 2.3.4. Determination of Enthalpy ( $\Delta H^*$ ) and Entropy ( $\Delta S^*$ ):

Enthalpy of activation ( $\Delta H^*$ ) and entropy ( $\Delta S^*$ ) were calculated using transition state theory equations (Eyring equation):

$$K = \frac{RT}{Nh} e^{\Delta S^*/R} \cdot e^{-\Delta H^*/RT} \quad (4)$$

where (K) is the rate constant, (N) is the Avogadro's number, (R) is the universal gas constant and h is planks constant.

By dividing the above equation by (T) and taking its natural logarithm, the following equation obtained:

$$\ln\left(\frac{k}{T}\right) = \ln\frac{R}{Nh} + \frac{(\Delta S^*)}{R} + \frac{(-\Delta H^*)}{RT} \quad (5)$$

A plot of  $\ln(k/T)$  against  $(1/T)$  is linear, with a slope equals to  $(-\Delta H^*/R)$  and intercept equals to  $(\ln. k/h + \Delta S^*/R)$ . Therefore  $(\Delta H^*)$  and  $(\Delta S^*)$  can be calculated from the slope and intercept, respectively [15,16].

#### 2.4. Elemental Analysis, Infrared and Ultraviolet Spectroscopy:

The carbon, hydrogen and nitrogen contents of the prepared polymer was carried out in the micro analytical laboratory at Cairo University by using oxygen flask combustion and a dosimat E415 titrator (Switzerland).

The infrared spectroscopic analysis of the prepared polymer at the investigated optimum condition was carried out in the micro analytical laboratory at Cairo University by using a Shimadzu FTIR-430 Jasco spectrophotometer by using KBr disc technique for the IR investigations.

The ultraviolet-visible absorption spectra of the monomer and the prepared polymer sample were measured using Shimadzu UV spectrophotometer (M 160 PC) at room temperature in the range 200-400 nm using dimethyl formamide as a solvent and reference.

#### 2.5. Thermal Gravimetric Analysis (TGA), Transmission Electron Microscopy (TEM) and X-Ray Analysis:

Thermal gravimetric analysis (TGA) of the polymer sample was performed using a SHIMADZU DT-30 thermal analyzer. The weight loss was measured from ambient temperature up to 600 °C at rate of 20 °C/ min to determine the rate of polymer degradation.

X-Ray diffractometer (philip1976.model1390) was used to investigate the phase structure of the polymer powder under the following condition which kept constant during the analysis processes: Cu: X-ray tube, scan speed =8/min, current=30mA, voltage =40kv and preset time=10s.

The inner cavity and wall thickness of the prepared polymer was investigated using transmission electron microscopy (TEM) JEOL JEM-1200 EX II (Japan).

#### 2.6. Dielectric properties and a.c conductivity Measurements:

The dielectric constant ( $\epsilon'$ ), the dielectric loss ( $\epsilon''$ ) and a.c conductivity ( $\sigma_{ac}$ ) were measured using Philips RCL bridge (digital and computerized) at a frequency range 12 - 10<sup>5</sup> Hz and over temperature range 30 - 60 °C

The values of the dielectric constant were determine using standard geometric technique in which the capacitance (C) was assumed to be given by the usual expression for a parallel plate capacitor. using the following:

$$\epsilon' = \frac{Cd}{\epsilon_0 A} \quad (6)$$

where ( $\epsilon'$ ) is the dielectric constant, ( $\epsilon_0$ ) is the permittivity of vacuum, A is the area of the sample and d is the sample thickness.

The dielectric loss ( $\epsilon''$ ) was calculated from the measurements of the loss factor (D) and ( $\epsilon'$ ) using the following relation:

$$\epsilon'' = D \epsilon' \quad (7)$$

The ac conductivity was measured using Philips RCL Bridge (digital and computerized) at a frequency range 0.1 - 100 k Hz and at temperature range 30 - 80 °C. The temperature was controlled by the use of a double wound electric oven.

The a.c conductivity ( $\sigma_{ac}$ ) value was calculated using the relation:

$$\sigma_{ac} = \epsilon'' \omega \epsilon_0 \quad (8)$$

where  $\omega = 2\pi f$  and f is the applied frequency.

#### 2.7 Method of calculations:

In this work DFT (B3LYP) [17,18]method was used. This functional is a combination of the Becke's three parameters non-local exchange potential with the non-local correlation functional of Lee et al. Full geometry optimization was performed using 6-311G (d,p) as a basis set to generate the optimized structures and ground state properties of p-toluidine, radical cation (monomer and dimer...etc.). All calculations were performed using Gaussian 09 W program [19].

### 3. Result and Discussion:

#### 3.1. Determination of the Optimum Polymerization Conditions:

The polymerization process of p-toluidine (pTO) occurs by using hydrochloric acid (HCl) as dopant and medium in the presence of potassium dichromate as initiator at 15±0.2 °C for one hour, using

constant total volume (25 ml). The obtained yield of the polymer was determined after drying under vacuum at  $60^{\circ}\text{C}$  until constant weight.

### 3.1.1. Effect of HCl Concentration

To study the effect of HCl concentration on the polymerization reaction, both oxidant ( $\text{K}_2\text{Cr}_2\text{O}_7$ ) and monomer concentrations were fixed at 0.1M but HCl concentration was varied from 0.1 M to 0.5 M at  $15\pm 0.2^{\circ}\text{C}$ . The relation between (PpTO) yield and different concentrations of HCl is represented in figure (1). From which it is clear that, the polymer yield increase with the increasing the acid concentration in the range from 0.1 to 0.3 then decreases gradually up to 0.5M.

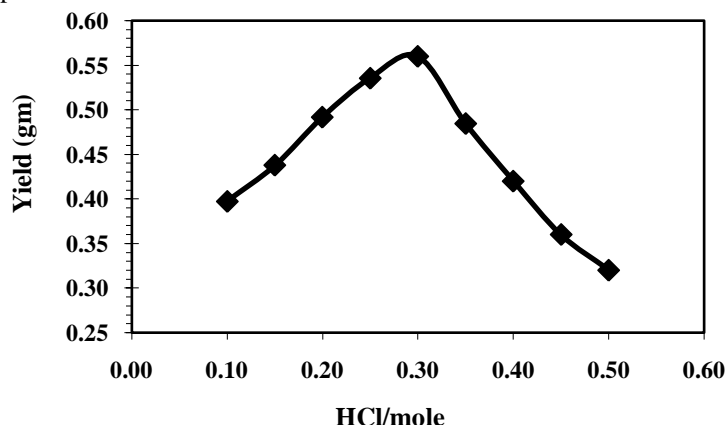


Figure (1): Yield - HCl concentration effect on the aqueous oxidative polymerization of (PpTO).

### 3.1.2. Effect of Potassium Dichromate Concentration

Both of the monomer and HCl concentrations are kept constant at 0.1 and 0.3 M respectively while the oxidant concentrations were varied from 0.1 to 0.5M at  $15\pm 0.2^{\circ}\text{C}$  to investigate the optimum polymerization condition of oxidant. Figure (2) shows the plot of p-toluidine polymer (PpTO) yield against different concentrations of the oxidant. The obtained yield increases with the increase of  $\text{K}_2\text{Cr}_2\text{O}_7$  concentration reaching to maximum value at 0.25M then decreases from 0.25M to 0.5M. In the first part of the curve the produced initiator ion radical moieties activate the backbone and consequently produce the p-toluidine (pTO) ion radical, which takes place immediately and therefore, the yield increases with the increase of potassium dichromate concentration up to 0.25M. But in the range from 0.25M to 0.5M the polymer yield decrease, may be due to at a high concentration of oxidant, it promotes the formation of low molecular weight oxidation product and also may be degrade the produced polymer which is easily soluble in acid medium [16,20].

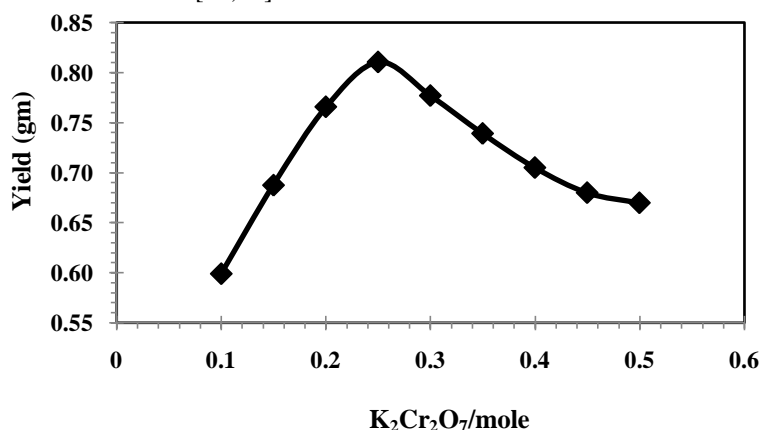


Figure (2): Yield -  $\text{K}_2\text{Cr}_2\text{O}_7$  concentration effect on the aqueous oxidative polymerization of (PpTO).

### 3.1.3. Effect of the Monomer Concentration:

To investigate the effect of monomer concentration on the polymerization reaction, both  $K_2Cr_2O_7$  and HCl concentrations were kept constant at 0.25 and 0.3 M respectively at  $15 \pm 0.2^\circ C$ . The obtained data shows that, the optimum yield of polymer was found in case of using monomer concentration equal to 0.3 M as shown in figure (3).

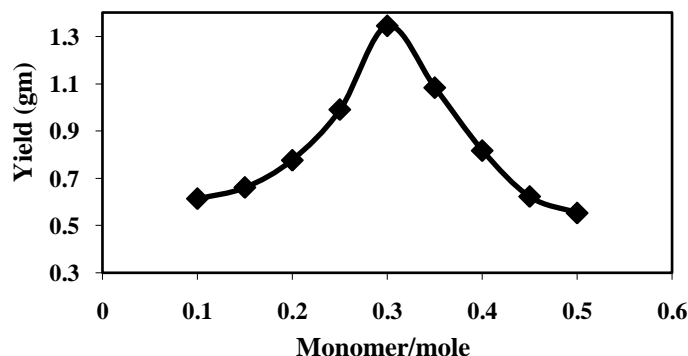


Figure (3): Yield - monomer concentration effect on the aqueous oxidative polymerization of (PpTO).

## 3.2: The kinetic Studies of the Polymerization Reaction

### 3.2.1: Effect of hydrochloric Acid Concentration

The kinetic study of aqueous oxidative polymerization for (pTO) was carried out using constant monomer concentration at (0.3 M) and  $K_2Cr_2O_7$  as oxidant at (0.25 M) using different molarities from HCl (0.05 - 0.3 mol/L) and constant total volume (25 ml) at  $15 \pm 0.2^\circ C$  for different time intervals. The yield-time curves were plotted for each acid concentration used as shown in figure (4-a). From which it is clear that, both the initial and overall reaction rates of the polymerization reaction increase with the increasing of HCl concentrations in the range between 0.05-0.3 mol/L. The HCl exponent was determined from the relation between logarithm of the initial rate of polymerization ( $\log(R_i)$ ) against logarithm of the HCl concentration as represented in figure (4-b). A straight line is obtained with a slope equal to 0.949, which means that the polymerization reaction is first order reaction with respect to HCl concentration.

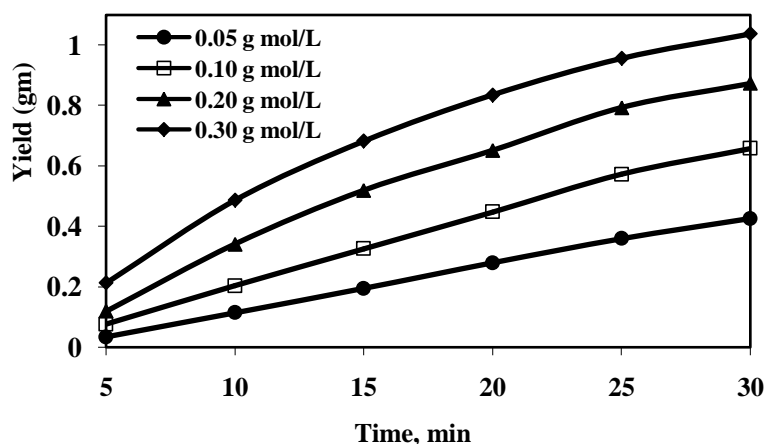
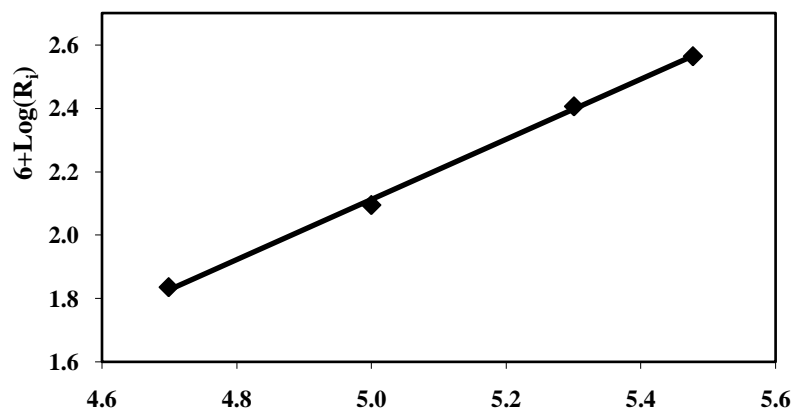


Figure (4-a): Yield -time curve for the effect of HCl concentration on the Polymerization of p-toluidine (pTO) at different time intervals.



### 6+Log (HCl)

Figure (4-b)-Double logarithmic plot of the initial rate and HCl concentration for the chemical oxidative polymerization of (pTO).

### 3.2.2: Effect of Potassium Dichromate Concentration

The effect of  $K_2Cr_2O_7$  on the aqueous oxidative polymerization of (pTO) was carried out at fixed concentrations of monomer at 0.3 M and HCl 0.3 M. The oxidant concentration was investigated in the range between 0.05-0.25 mol/L using constant total volume (25 ml) at  $15 \pm 0.2^\circ C$  for different time intervals. The yield-time curves were plotted for different oxidant concentrations and the data are graphically represented in figure (5-a). The initial and overall reaction rates were determined using equation (2). Figure (5-a) shows that, the initial and overall reaction rate of the polymerization reaction increases with the increase of oxidant concentration in the range between 0.05 - 0.25 mol/l. The oxidant exponent was determined from the relation between logarithm of the initial rate of polymerization ( $\log(R_i)$ ) against logarithm of the oxidant concentration. A straight line was obtained with a slope of 0.982 as represented in figure (5-b). This means that the polymerization reaction of (pTO) is a first order reaction with respect to the oxidant.

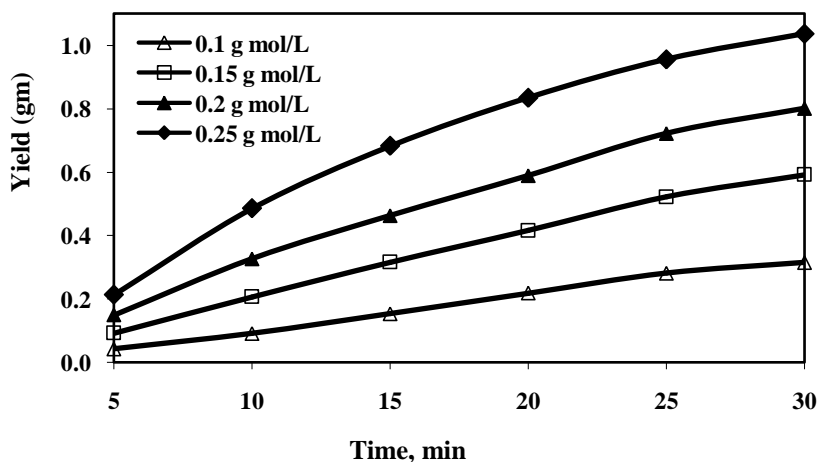


Figure (5-a): Yield-time curve for the effect of potassium dichromate concentration on the polymerization of (pTO) at different time intervals.

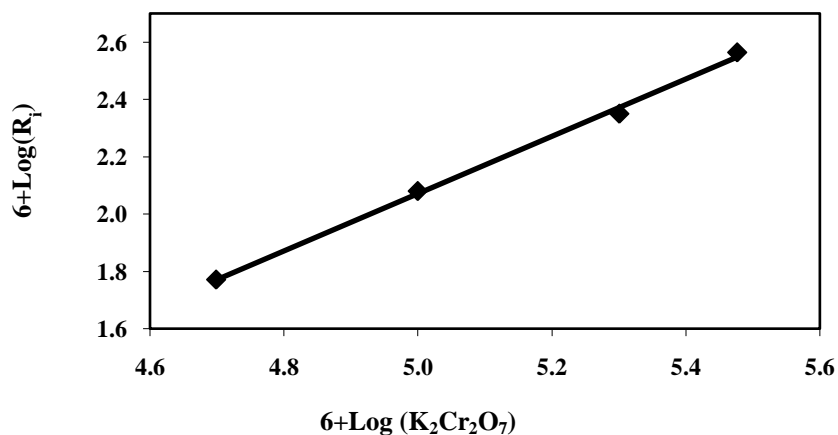


Figure (5-b): Double logarithmic plot of the initial rate and oxidant concentration in case of polymerization of (pTO).

### 3.2.3: Effect of Monomer (pTO) Concentration:

The effect of monomer concentration on the aqueous oxidative polymerization of pTO is investigated by using different concentration of monomer (0.05-0.3 mol/L) at constant volume 25 ml. The HCl solution and potassium dichromate concentrations were fixed at 0.3 and 0.25 M respectively at  $15 \pm 0.2$  °C for different time intervals. The yield-time curve is plotted for each monomer concentration and the data are graphically represented in figure (6-a). The monomer exponent was determined from the slope of the straight line represented in figure (6-b) for the relation between  $\log R_i$  and logarithm of the monomer concentration. The slope of this linear relationship is found to be 1.12 which means that the polymerization reaction with respect to the monomer concentration is a first order reaction.

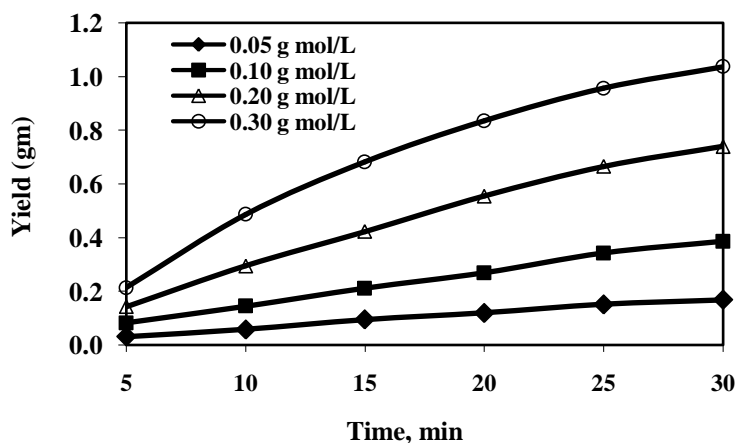


Figure (6-a): Conversion - monomer/mol concentration effect on the aqueous oxidative polymerization of (pTO) at different time intervals

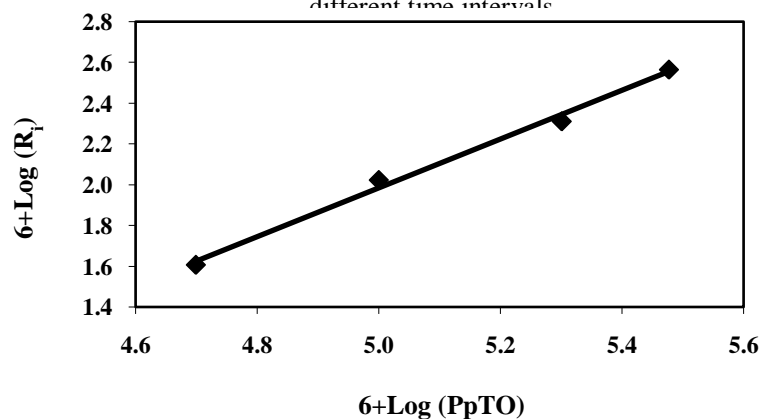


Figure (6-b)-Double logarithmic plot of the initial rate and monomer concentration of (pTO).

### 3.3: Calculation of the Thermodynamic Activation Parameters:

The aqueous oxidative polymerization of 0.30 mol/L (pTO), 0.3 mol/L HCl and 0.25 mol/L potassium dichromate as oxidant was carried out at 5, 10 and 15 °C for different time intervals. The yield- time curves were plotted in figure (7), from which it is clear that both of the initial and overall reaction rates increase with raising the reaction temperature. The apparent activation energy ( $E_a$ ) of the aqueous polymerization reaction was calculated using equation (6). The apparent activation energy for this system was found to be 79.04 kJ/mol. The enthalpy and entropy of activation for the polymerization reaction can be calculated by the calculation of  $K_2$  from the following equation:

$$\text{Reaction Rate} = K_2 [\text{oxidant}]^{0.982} [\text{HCl}]^{0.949} [\text{monomer}]^{1.197} \quad (9)$$

The values of  $K_2$  at 5, 10 and 15 °C were  $3.63 \times 10^{-6}$ ,  $6.66 \times 10^{-6}$  and  $11.91 \times 10^{-6}$  respectively. The enthalpy ( $\Delta H^*$ ) and entropy ( $\Delta S^*$ ) of activation associated with  $K_2$ , were calculated using Eyring equation (4).

Where  $K_2$  is the rate constant,  $N$  is the Avogadro's number,  $R$  is the universal gas constant and  $h$  is planks constant.

Figure (9) shows the relation between  $K_2/T$  vs  $1/T$ , which gives a linear relationship with slope equal to  $(-\Delta H^*)/R$  and intercept equal to  $(\log R/Nh + \Delta S^*/R)$ . From the slope and intercept, the values of  $\Delta H^*$  and  $\Delta S^*$  are calculated and found to be equal to  $76.68 \text{ kJmol}^{-1}$  and  $-80.52 \text{ Jmol}^{-1}\text{K}^{-1}$  respectively.

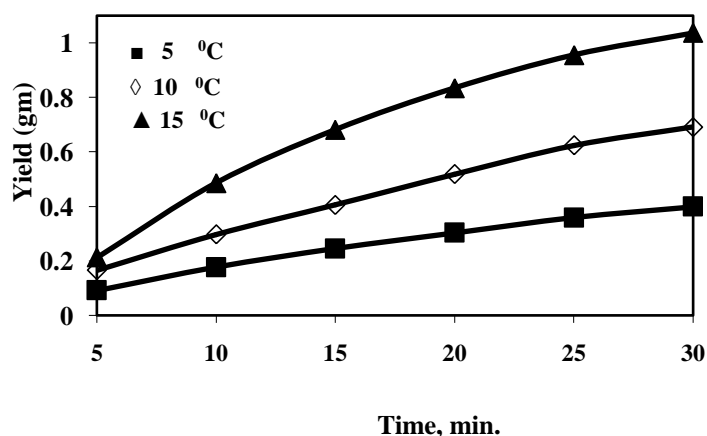


Figure (7): Yield -time curve for the effect of temperature on the aqueous oxidative polymerization of (pTO).

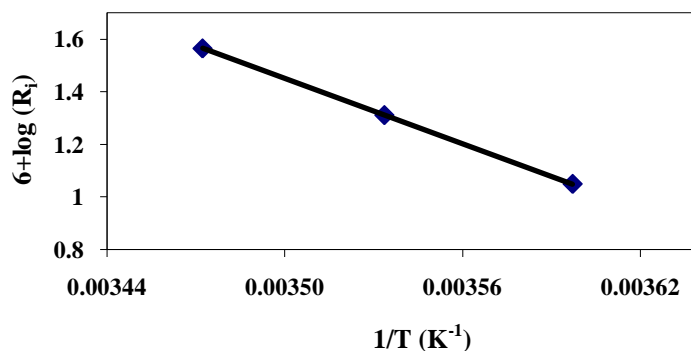


Figure (8): The relation between the logarithm of initial rate and  $(1/T)$  for aqueous oxidative polymerization of (nTO).

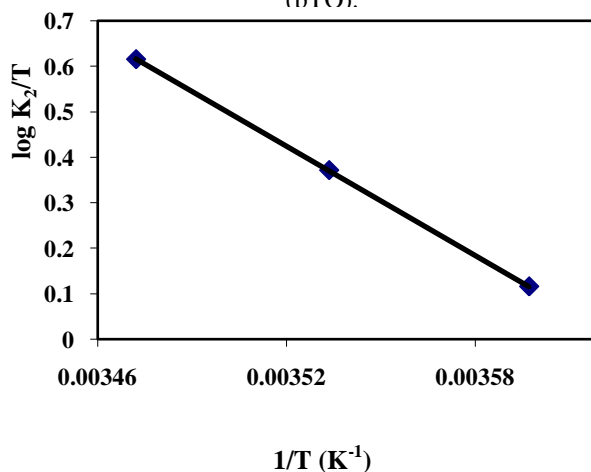


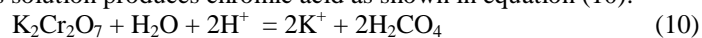
Figure (9): The relation between  $\log K_2/T$  and  $1/T$  for the polymerization reaction of (pTO).

### 3.4 Polymerization Mechanism.

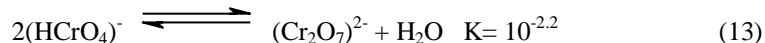
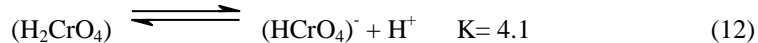
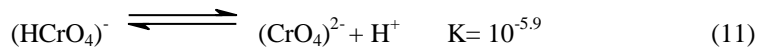
The aqueous oxidative polymerization of (pTO) is described in the Experimental section and follows three steps [16,20]:

#### *The Initial Step*

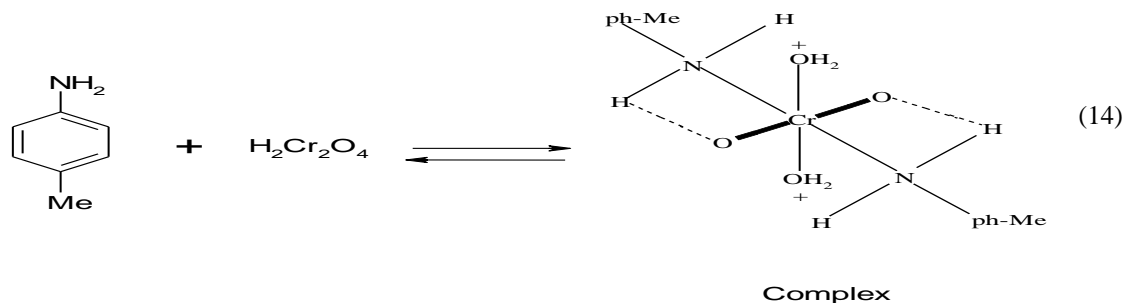
Potassium dichromate in acidified aqueous solution produces chromic acid as shown in equation (10):



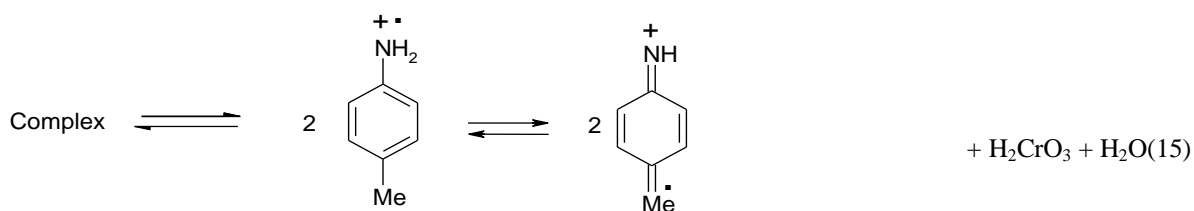
This reaction is controlled by the change in pH, the orange red dichromate ions  $(\text{Cr}_2\text{O}_7)^{2-}$  are in equilibrium with the  $(\text{HCrO}_4^-)$  in the range of pH-values between 2 and 6, but at pH below 1 the main species is  $(\text{H}_2\text{CrO}_4)$  and the equilibrium can occur as follows:



The chromic acid withdraws one electron from each protonated OMA and probably forms a metastable complex as shown in equation (15):



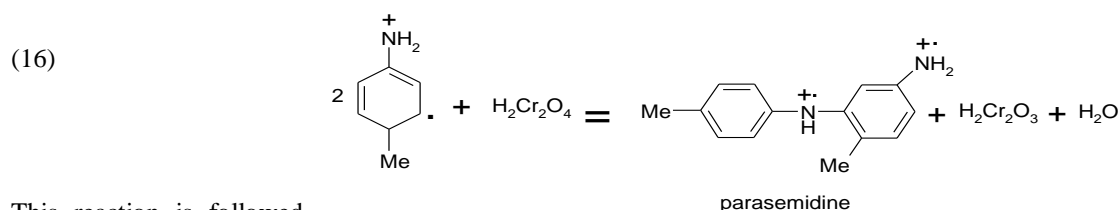
The complex undergoes dissociation to form monomer cation radical as shown in equation (15):



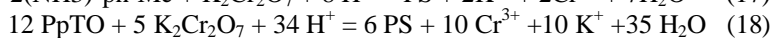
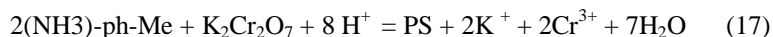
Generally, the initial step is rapid and may occur in short time, 0–5 min (autocatalytic reaction).

#### **Propagation Step:**

This step involves the interaction between the formed radical cation and the monomer to form a dimer radical cation. In the case of Cr (VI) oxidation of the organic compounds, Cr (VI) is reduced to Cr (IV) first and then to Cr (III) [16,20]. Transfer of two electrons from two monomer ion radical by  $\text{H}_2\text{CrO}_4$  produces parasemidine salt along with chromous acid  $\text{H}_2\text{CrO}_3$  (Cr (IV)). The intermediately produced Cr (IV) oxidizes parasemidine to permigraniline salt (PS) at suitable low pH and the PS acts as a catalyst for conversion of p-toluidine to poly-p-toluidine. In case of PpTO the para position is busy so, the polymerization occurs in the meta position.

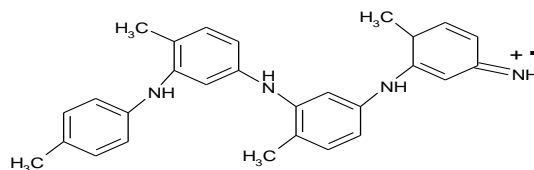


This reaction is followed by further reaction of the formed dimer radical cations with other monomer molecules to form trimer radical cations and so on. The degree of polymerization depends on different factors such as oxidant concentration, HCl concentration, monomer concentration, and temperature. By adding equations 10, 13, 14, 15 and 16.



#### **Termination Step**

Termination of the reaction occurs by the addition of ammonium hydroxide solution in an equimolar amount to HCl present in the reaction medium (till pH = 7), which leads to stop of the redox reaction. The reaction could occur as follows:



### 3.5 DFT Calculations:

From the polymerization mechanism see (Section 3.4), the radical cation formed in the initial step (0-5 min) followed by the propagation step involves the interaction between the formed radical cation and the monomer to form a dimer radical cation. This reaction is followed by further reaction to form the polymer chain. In this section we by theoretically calculation explain why radical cation start the polymerization and not the neutral monomer of p-toluidine and at the same time explore the stability of the dimer radical cation if it is (ortho – attack) or (meta – attack) in the propagation steps.

#### 3.5.1 Monomer and radical cation (initiation):

The final optimized geometry, numbering system, the vector of the dipole moment, the equilibrium bond length and net charge on active center of neutral monomer and radical cation of p-toluidine using DFT – B3LYP/ 6-311G\*\* are present in figure (10 and 11). Table (1) present the total energy ( $E_T$ ),  $E_{HOMO}$ ,  $E_{LUMO}$ , energy gap ( $E_g$ ) and dipole moment of neutral and radical cation of p-toluidine.

Table (1): The total energy, energy of HOMO and LUMO, energy gap and vector of the dipole moment of the monomer and the radical cation of (PTO).

Parameter	Monomer	Radical cation
$E_T$ (a.u)	-327.0143	-326.7484
$E_{HOMO}$ (a.u)	-0.20548	-0.40972
$E_{LUMO}$ (a.u)	-0.01281	-0.33128
$E_g$ (eV)	5.2429	2.1345
Total $\mu$	1.4633	3.3322

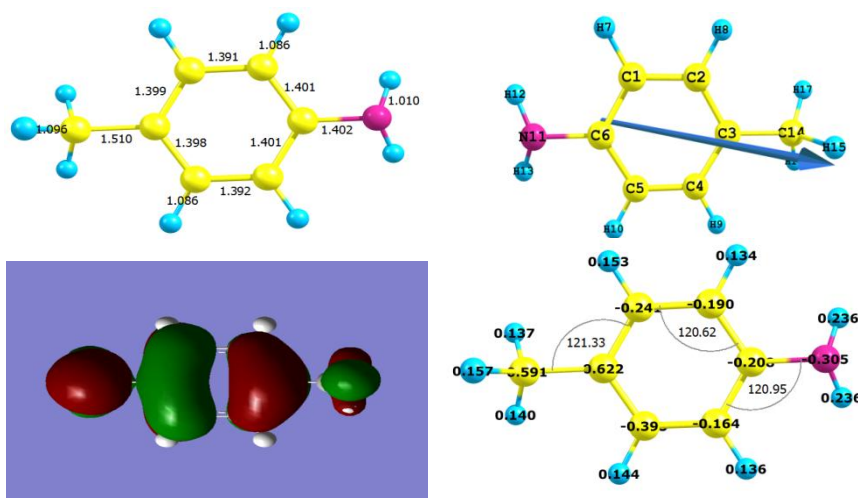


Figure (10): Geometry optimization, numbering system, vector dipole moment, bond length, net charge and HOMH charge density of the monomer (PTO).

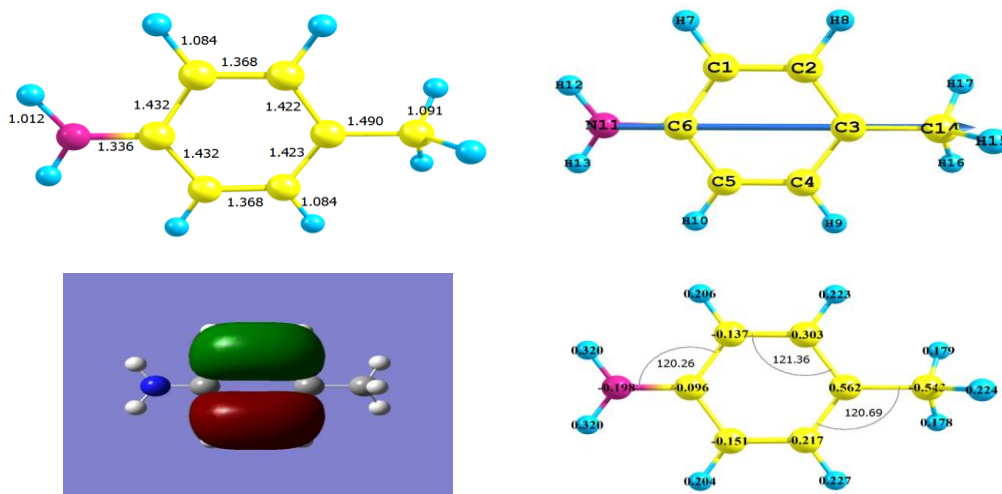


Figure (11): Geometry optimization, numbering system, vector dipole moment, bond length, net charge and HOMH charge density of (pTO) radical cation.

***Some general remarks can be considered:***

- 1- The computed total energy of radical cation is less stable than neutral monomer by 7.06 eV (162.8 Kcal), indicating that the radical cation is more reactive than neutral monomer.
- 2- The computed energy gap ( $E_g$ ), which measures the reactivity. As the energy gap decreases, the reactivity increases. In our case, the  $E_g$  of radical cation is less than the neutral monomer by 3.06 eV (70.7 Kcal), this is a second reason why radical cation is more reactive and starts the process of polymerization.
- 3- From the computed dipole moment, it is found that the dipole moment of radical cation is greater than the neutral monomer by 1.86 D.
- 4- The net charge on N-atom of amino group in neutral monomer is -0.305 e, whereas, in radical cation it is -0.198 e. The decrease in negativity of N-atom of amino group is another reason for this center to attack the ortho- or meta- position of the neutral monomer to start polymerization as indicated in HOMO charge density map (Fig. 10, 11).

**3.5.2 Propagation step:**

The next step of the polymerization is the propagation step at which the radical cation attacks another monomer to form the dimer radical cation.

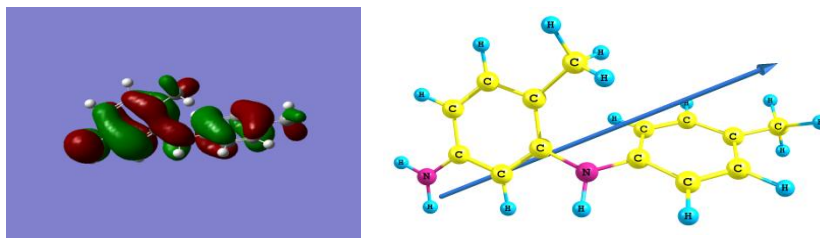
To prove which position in the monomer is attacked by the radical cation to form the dimer radical cation, we calculate the total energy of the dimer radical cation at B3LYP/6-311G\*\* method. Fig. (12) presents the final geometry, the vector of the dipole moment, total energy and energy gap and HOMO charge density maps. Two possible structures may be considered: dimer radical cation (ortho- attack) and dimer radical cation (meta-attack). From Fig. (12) one can reveal the following:

- 1- The computed total energy (which measures the stability of any compound) of dimer radical cation (meta-attack) is less (more stable) than dimer radical cation (ortho-attack) by 5.77 eV (133 kcal). This means that in the reaction medium dimer radical cation (meta-attack) is predominant over dimer radical cation (ortho-attack).
- 2- Another reason why dimer radical cation (meta-attack) is more reactive than (ortho-attack) is the energy gap, as the energy gap decreases, the reactivity increases. Dimer radical cation (meta-attack) is more reactive than dimer radical cation (ortho-attack) by 0.323 eV (7.4 kcal). From the above, one can conclude that in the initiation process, the radical cation is more stable than monomer and dimer radical cation (meta-attack) is more stable than dimer radical cation (ortho-attack) in the propagation process.

Dimer radical cation (meta-attack) interacts with another monomer to form trimer and so on to form polymer chain scheme (1).

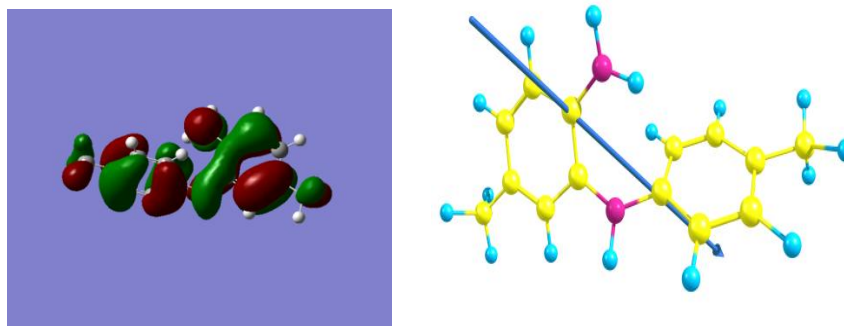
**Dimmer**

**1- The meta-position**



$E_T$  (a.u) = -652.4351,  $E_{HOMO}$  (a.u) = -0.3326,  $E_{LUMO}$  (a.u) = -0.2822,  $E_g$  (eV) = 1.3706 and Total  $\mu$  = 4.1210

## 2- The ortho-position:



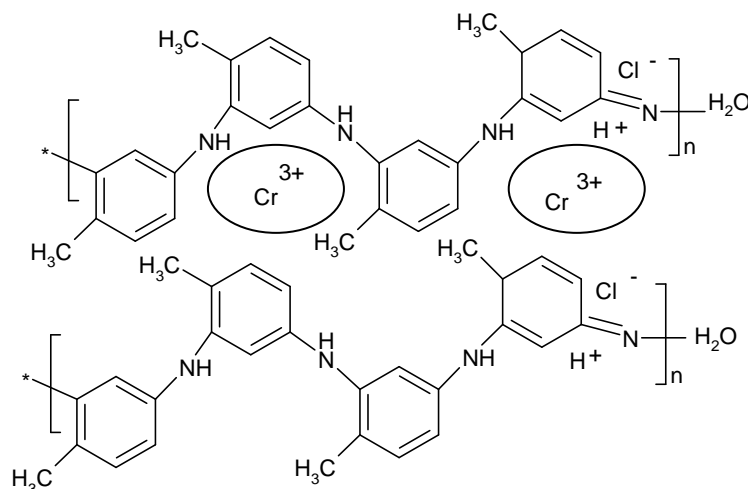
$E_T$  (a.u) = -652.2598,  $E_{HOMO}$  (a.u) = -0.3407,  $E_{LUMO}$  (a.u) = -0.2785,  $E_g$  (e.v) = 1.6941 and Total  $\mu$  = 1.9643

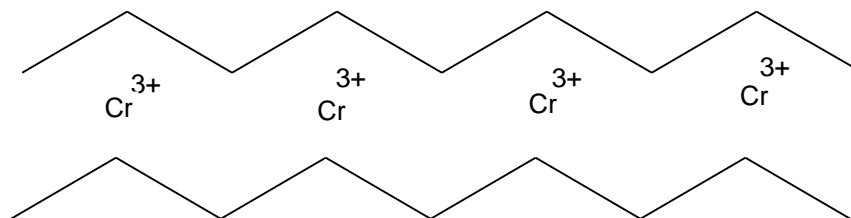
Figure (12): Geometry optimization, vector dipole moment and HOMH charge density of ortho- and meta-position of the dimmer.

## 3.6. Characterization of the Obtained Polymer:

### 3.6.1. The Elemental Analysis:

The data obtained from elemental analysis using oxygen flask combustion and a dosimat E415 titrator which are given in table (2) shows that, the found carbon content of (PpTO) is lower than the calculated value. This is due to the formation of chromium carbide during step of heating and measuring process while the found value of nitrogen and hydrogen are 8.84 and 4.56 respectively which are in good agreement with the calculated one for the suggested structure present in scheme (1). By measuring another sample of the (PpTO) which was prepared by using ammonium persulfate as oxidant the found value of carbon, is higher than sample which, is prepared by using potassium dichromate as oxidant [16,21].





Scheme (1).Structure of the prepared poly p-toluidine (PpTO)

Table (2): The elemental analysis of poly-P-tolidine (PpTO).

C %		N %		H %	
Calc.	Found	Calc.	Found	Calc.	Found
57.98	33.35	9.65	8.84	5,68	4.56

### 3.6.2. The infrared spectroscopic analysis of (PpTO) monomer and its analogs polymer:

The IR spectra of the p-toluidine and its polymer (PpTO) are represented in Figure (13), while the absorption band values and their assignments are summarized in Table (3). The sharp absorption band appearing at  $504\text{ cm}^{-1}$  which could be attributed to the bending deformation of N-H group attached to benzene ring in case of monomer, appears as broad absorption band at  $505\text{ cm}^{-1}$  with slight shift in case of polymer. The shoulder absorption band appearing at  $761\text{ cm}^{-1}$  which could be attributed to out of plane deformation of CH for 1,4-disubstituted benzene ring in case of monomer but disappears in case of polymer. The strong absorption band appearing at  $811\text{ cm}^{-1}$  due to the rocking deformation of methylene group in case of monomer, appears at  $814\text{ cm}^{-1}$  with slight shift in case of polymer. A series of absorption bands appearing in the region from  $1049 \dots 1269\text{ cm}^{-1}$  which could be attributed to symmetric stretching vibration for C-N groups in both cases (monomer and polymer). The sharp splitted band appears at  $1451, 1624\text{ cm}^{-1}$  in case of monomer and the corresponding broad absorption bands appearing at  $1445\text{ cm}^{-1}$  and  $1575\text{ cm}^{-1}$  in case of polymer are attributed to stretching vibration for C=C in benzene ring of quinoid unit. The three medium bands appearing at  $2858, 2910$  and  $3013\text{ cm}^{-1}$  which could be attributed to hyper conjugation in case of the monomer disappears in case of the polymer. The two shoulder and broad bands appear at  $3336$  and  $3415\text{ cm}^{-1}$  in case of the monomer, appears as a broad band at  $3405\text{ cm}^{-1}$  in case of polymer.

Figure (13): The infrared spectrum of pTO (a) and its polymer(b).

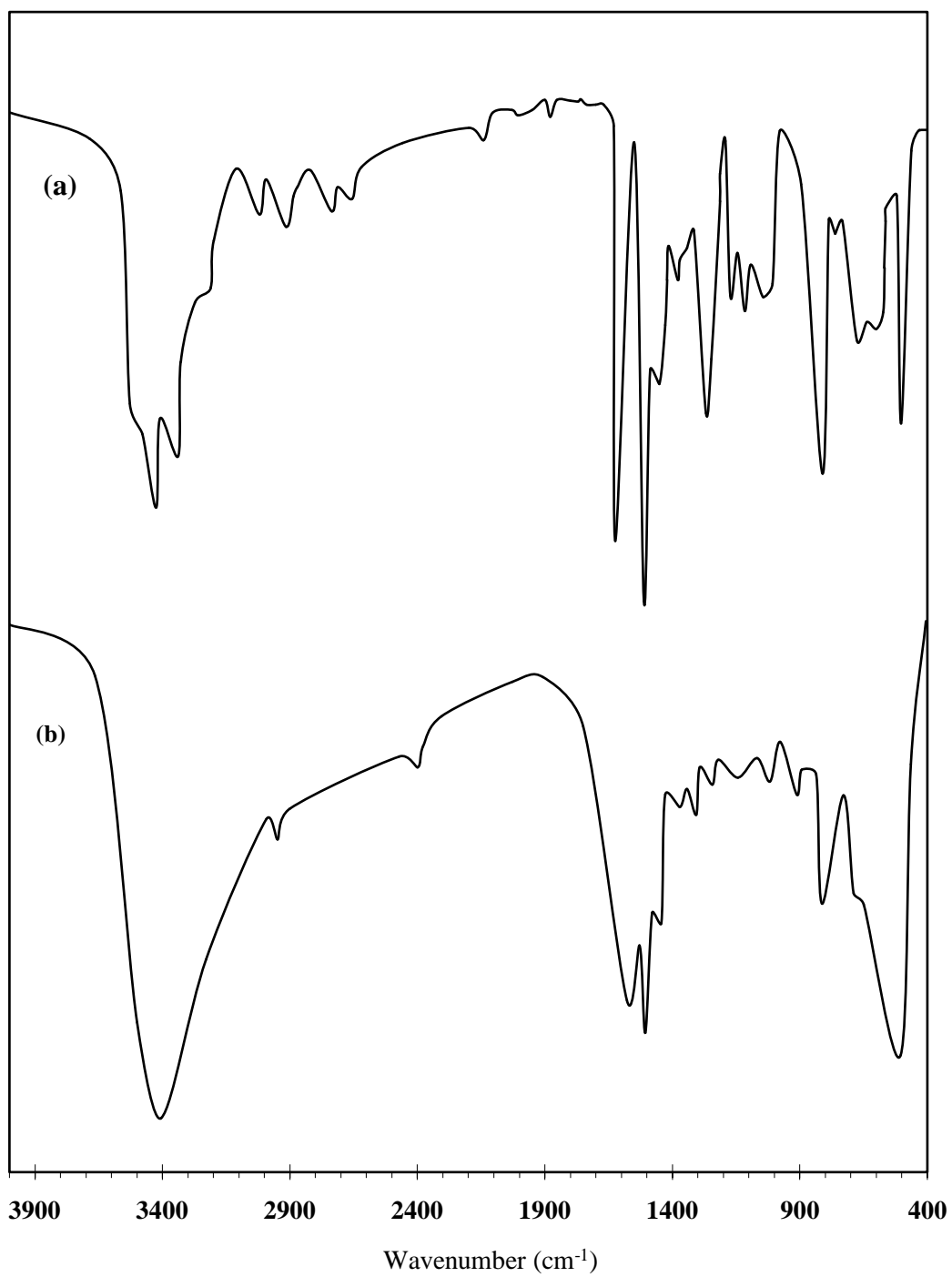


Table (3): Infrared absorption bands and their assignments of p-tolidine monomer and its analogs polymer.

Wave number( $\text{cm}^{-1}$ )		Assignments
Monomer	Polymer	
504 <sup>s</sup>	411 <sup>w</sup>	Bending deformation of N-H group attached to benzene ring
677 <sup>b</sup>	505 <sup>b</sup>	
761 <sup>w</sup>	—	Out of plane C-H deformation of 1,2-disubstitution of benzene ring, in case of monomer and 1,2,4 tri-substituted of benzene ring, in case of polymer.
811 <sup>s</sup>	—	
—	814 <sup>s</sup>	
850 <sup>w</sup>	—	
—	860 <sup>w</sup>	
1049 <sup>m</sup>	1018 <sup>w</sup>	Out of plane C-H deformation of 1,4-disubstitution of benzene ring
1117 <sup>m</sup>	1110 <sup>w</sup>	
1173 <sup>m</sup>	1163 <sup>w</sup>	
—	1248 <sup>w</sup>	Symmetric stretching vibration for C-O and C-N groups
1269 <sup>s</sup>	—	
1451 <sup>sh</sup>	1307 <sup>w</sup>	Stretching vibration for C=C in aromatic system
1512 <sup>s</sup>	1445 <sup>sh</sup>	
—	1509 <sup>s</sup>	
1624 <sup>s</sup>	1575 <sup>b</sup>	Symmetric stretching vibration of N-H
1875 <sup>w</sup>	—	
2371 <sup>w</sup>	2341 <sup>w</sup>	Stretching vibration of C-H aromatic
2858 <sup>m</sup>	—	
2910 <sup>m</sup>	2920 <sup>w</sup>	
3013 <sup>m</sup>	—	Asymmetric stretching vibration for NH group
3336 <sup>sh</sup>	—	
—	3405 <sup>b</sup>	
3415 <sup>b</sup>	—	

s= sharp

m= medium

w=weak

b=broad

sh=shoulder

### 3.6.3. The UV-visible Spectroscopic Study of p-p-tolidinemonomer and its analogs polymer:

The UV-visible spectra of p-methylaniline and its polymer are represented in Figure (14); the spectra show the following absorption bands:

In case of monomer, two absorption bands appear at  $\lambda_{\max} = 252$  and  $294$  nm which may be attributed to  $\pi-\pi^*$  transition (E2-band) of the benzene ring and the  $\beta$ -band (A1g – B2u).

In case of polymer, the absorption band appear: at  $\lambda_{\max} = 242$  nm which may be attributed to  $\pi-\pi^*$  transition showing a bathochromic shift. Beside this band, broad absorption band appears in the visible region at  $\lambda_{\max} = 432$  nm which may be due to the high conjugation of the aromatic polymeric chain.

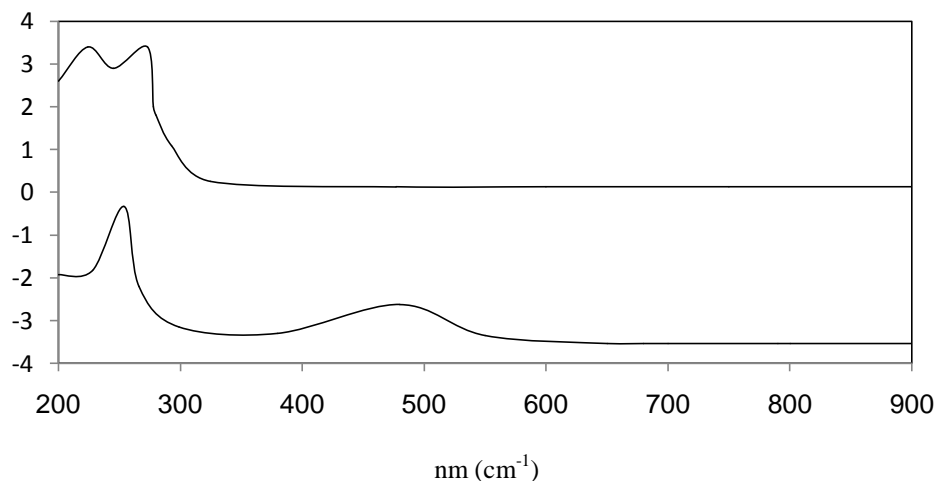


Figure (14): UV-visible spectra of p-tolidine (pTO) (A) and its analogous polymer (PpTO) (B).

### 3.6.4. Thermal Gravimetric analysis (TGA) of poly p-tolidine :

Thermogravimetric analysis (TGA) for the prepared polymer has been investigated and the TGA-curve is represented in Figure (15). The calculated and found data for the prepared polymers are summarized in table (5). The thermal degradation steps are summarized as follows:

(1) The first stage includes the loss of one water molecule in the temperature range between 25.5-147.°C the weight of loss of this step was found to be 3.06 % which is in a good agreement with the calculated one (3.09%).

(2) The second stage, in the temperature range between 147.-235.6 °C the weight loss was found to be 6.30 %, which could be attributed to the loss of HCl molecule. The found weight loss is in good agreement with the calculated one (6.20 %).

(3) The third stage, in the temperature range between 235.6-350.5 °C, the weight loss was found to be 21.07 %, which is attributed to the loss of four molecules of  $\text{CH}_3$ . The calculated weight loss of this stage is equal to 21.07 %.

(4) The fourth stage, in the temperature range between 350.5-499.46 °C, the weight loss was found to be 17.66 %, which is attributed to the loss of one molecule of  $\text{C}_6\text{H}_3\text{-2NH}$ . The calculated weight loss of this stage is equal to 17.85 %.

(6) The last stage, above 499.46 °C, the remained polymer molecule was found to be 51.87 % including the metallic residue but the calculated one was found to be 52.06 %.

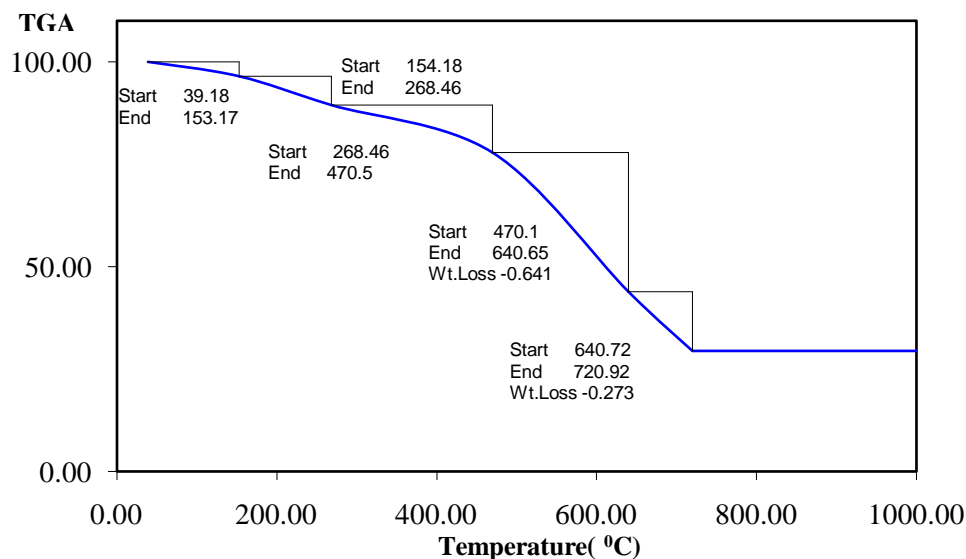


Figure 15: The thermal gravimetric analysis (TGA) for (PpTO)

**Table (4): Thermogravimetric data of PpTO.**

Name	Temperature range °C	Weight loss (%)		The removed molecule
		Calc.	Found	
Poly (pTO)	25.5-147	3.09	3.06	H <sub>2</sub> O
	147-235.6	6.30	6.30	HCl
	235.6-350.5	21.07	21.07	4CH <sub>3</sub>
	350.5-499.5	17.66	17.85	C <sub>6</sub> H <sub>3</sub> +2NH
	remaining weight(%) above 499.46	51.87	51.87	Remaining weight and metallic residue

### 3.6.5 -The X-Ray diffraction analysis and transimention electron microscope:

The X-Ray diffraction Patterns of the prepared polymer is represented in figure (16). The figure shows that, the prepared PpTO is completely amorphous.

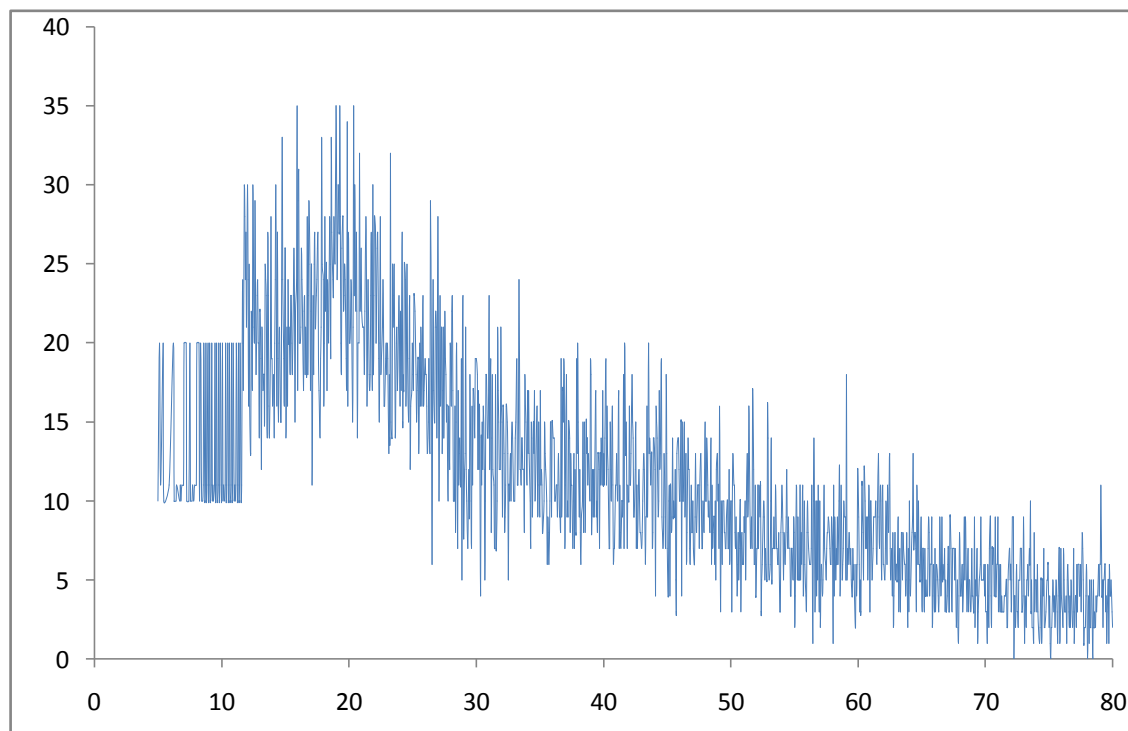


Figure 16: X-ray poly- p-tolidine (PpTO).

Morphology of PpTO was characterized by transmission electron microscope. Figure (17) shows TEM image of PpTO which shows spherical irregular shape with approximate diameter 76.05-153.70 nm either separated or linked with each other.

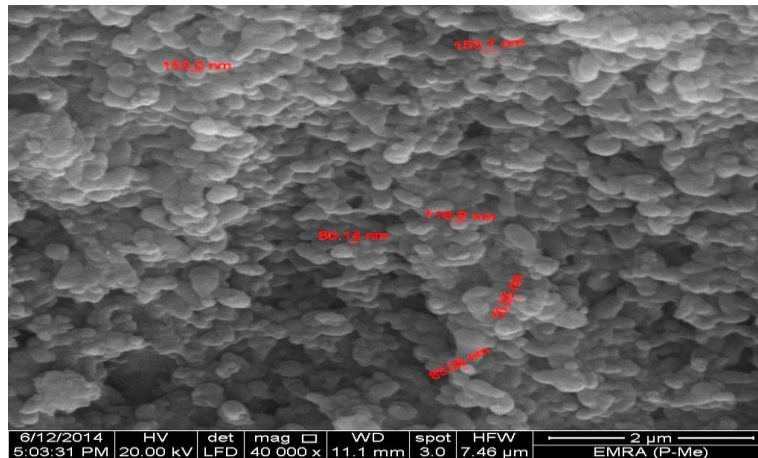


Figure (17): The transmission electron microscope of PpTO

### 3.7. Dielectric properties and a.c conductivity ( $\sigma_{ac}$ ) measurements:

Figure (18) show the variation in dielectric constant ( $\epsilon'$ ) of PpTO as a function of frequency. From the figure it is clear that, the dielectric constant decrease sharply up to a certain frequency after which becomes nearly constant. This behavior has also been observed by Rahaman, M, Sohi, N [22,23] and Pant, H.C[24]. This phenomenon could be attributed to relaxation process due to rotational displacement of molecular dipole under the influence of alternating filed which lead to dielectric relaxation. Consequently, decrease in dielectric constant may be due to the contribution of orientation relaxation of dipoles and conduction of charge carriers at higher frequency [25]. This can be explained on the basis of the fact that at close to high frequency, field reversal becomes so fast that dipoles are unable to orient themselves and intrawell hopping probability of charge carriers dominates in rapid field reversal in such a small interval of time [26].

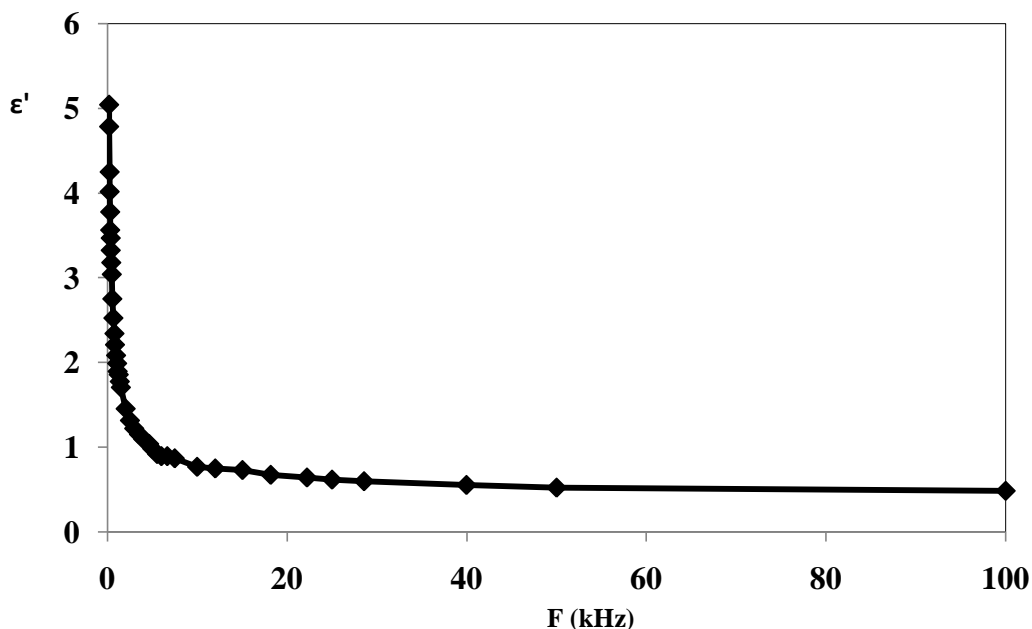


Figure (18): Variation of dielectric constant ( $\epsilon'$ ) of PpTO with frequency at room temperature.

Figure (19) reveals that dielectric loss  $\epsilon''$  decrease with the increasing of frequency. A decrease of  $\epsilon''$  orders of magnitude was observed when the frequency was increased from 0.1 kHz to 100 kHz. At low frequency, the high value of dielectric loss  $\epsilon''$  is usually associated with the motion of free charge carriers within the material, dipole polarization or interfacial polarization [26]. At high frequency, periodic field reversal is so fast that there is no excess ion diffusion in the direction of electric field and thus, charge accumulates and polarization decreases due to accumulation of charges leading to the decrease in  $\epsilon''$  [25,27].

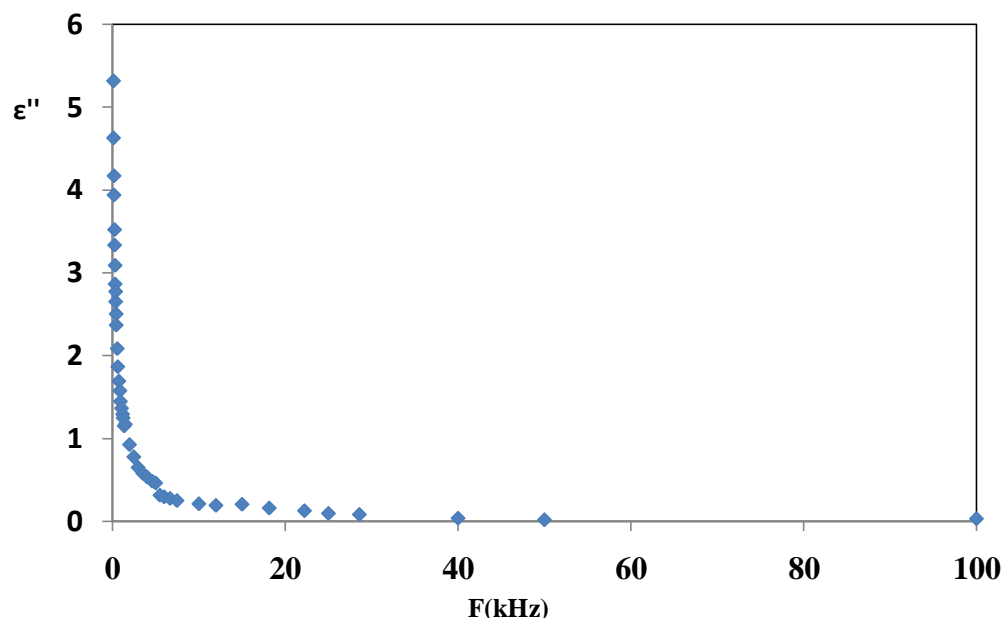


Figure (19): Variation of dielectric loss ( $\epsilon''$ ) of PpTO with frequency at room temperature.

Figure (20) represents the variation in ac conductivity ( $\sigma_{ac}$ ) for (PpTO) as a function of frequency and temperature. It is observed that, the value of ac conductivity increases with the increase of frequency. This behavior is in good agreement with the random free energy model proposed by Dyre, J. C., [25]. According to this model, conductance increases as a function of frequency in many solids, including polymers, which can be explained on the basis of any hopping model. The rise in conductivity upon increasing the frequency and temperature is common for disordered conducting polymer. As can be seen, each curve displays a conductivity dispersion, which is strongly dependent on frequency and shows weaker temperature dependent.

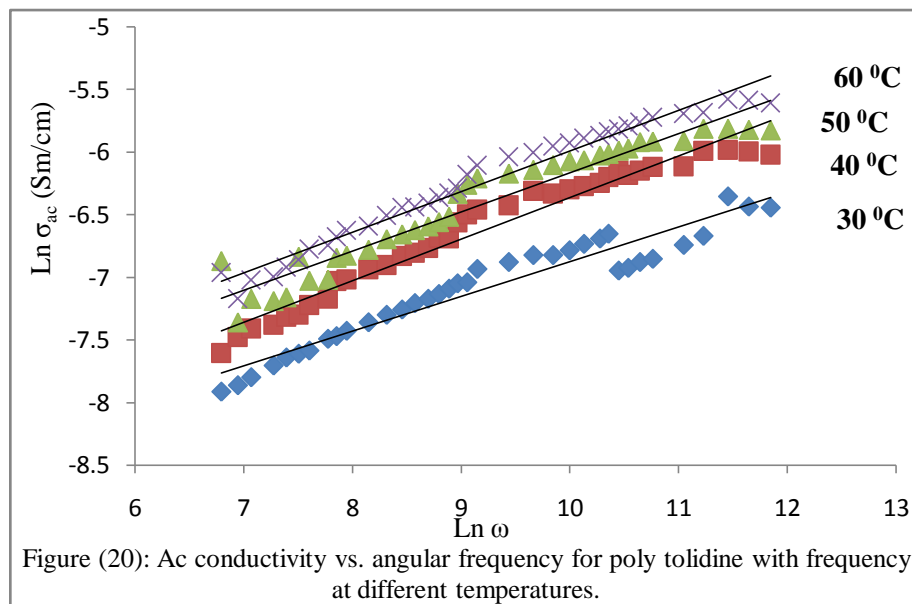


Figure (20): Ac conductivity vs. angular frequency for poly tolidine with frequency at different temperatures.

In general, for amorphous conducting material, disordered systems, low mobility polymers and even crystalline materials, the ac conductivity ( $\sigma_{ac}$ ) as a function of frequency can be obeys a power law with frequency [28]. The ac conductivity ( $\sigma_{ac}$ ) over a wide range of frequencies can be expressed as:

$$\sigma_{ac}(\omega) = A\omega^s \quad (17)$$

Where A is a complex constant and the index (s) is frequency exponent and  $\omega$  is the angular frequency ( $\omega = 2\pi f$ ).

Figure (20) shows the relation between  $\ln \sigma_{ac}$  and  $\ln \omega$  at different temperatures. The value of (s) at each temperature has been calculated from the slope of  $\ln \sigma(\omega)$  versus  $\ln(\omega)$  plot. As shown in figure (21) the calculated value of (s) for (PpTO) sample is less than unity. The microscopic conduction mechanism of disordered systems are governed by two physical processes such as classical hopping or quantum mechanical tunneling of charge carries over the potential barrier separating two energetically favorable centers in a random distribution. The exact nature of charge transport is mainly obtained experimentally from the temperature variation of exponent (s)[29]. The temperature exponent (s) dependences for (PpTO) sample reveals that the frequency exponent (s) decreases with the increase of temperature. This behavior is only observed in the correlated barrier hopping model proposed by Elliott, S.[30].

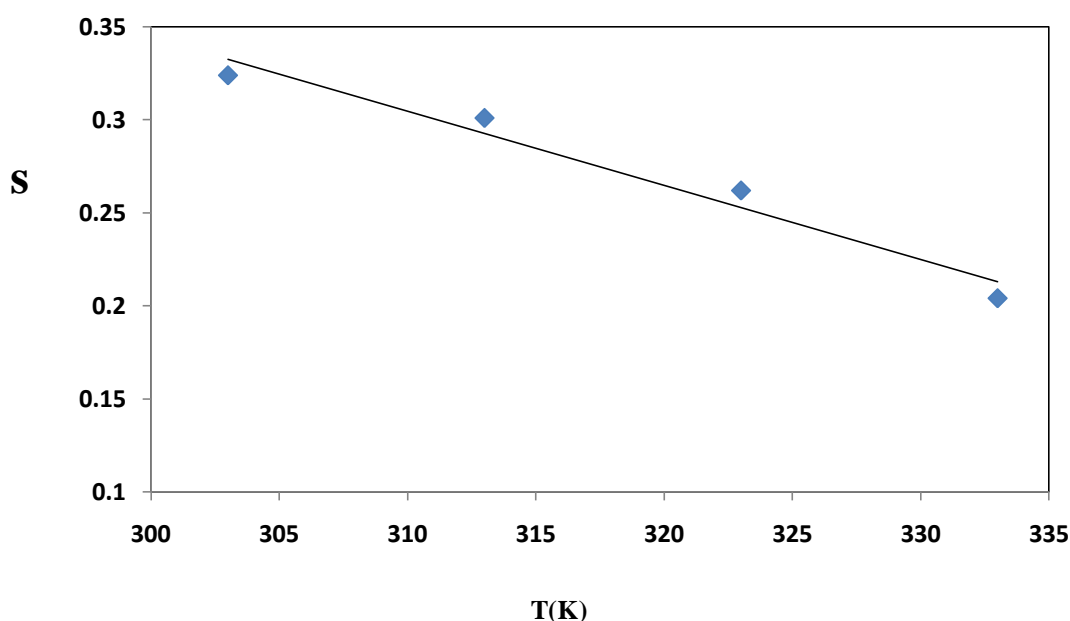


Figure (21 ):Frequency exponent (s) vs. temperature for poly tolidine.

## References

- [1] Prof. Sir. C.V. Raman Road, Bangalore et al., "Chemical and electrochemical polymerization of aniline using tartaric acid" European polymer journal 37 (2001), India
- [2] Jeevanada T, Siddaramaiah, Annadurai V, Somashekar R (2001) J ApplolymSci 82:383.
- [3] Liang L, Liu J, Windisch CF, Exarhos GJ, Lin Y (2002) AngewChemInt Ed 41:3665
- [4] P. C.Wang, L. H. Liu, D. A. Mengistie et al., "Transparent electrodes based on conducting polymers for display applications," Displays, vol. 34, no. 4, pp. 301– 314, 2013.

- [5] L. Wang, E.Hua, M. Liang et al., "Graphene sheets, polyaniline and AuNPs based DNA sensor for electrochemical determination of BCR/ABL fusion gene with functional hairpin probe," *Biosensors and Bioelectronics*, vol. 51, pp. 201–207, 2014.
- [6] M. Jaymand, "Recent progress in chemical modification of polyaniline," *Progress in Polymer Science*, vol. 38, no. 9, pp. 1287–1306, 2013.
- [7] Y. Cao, P. Smith, and A. Heeger, "Counter-ion induced processibility of conducting polyaniline and of conducting polyblends of polyaniline in bulk polymers," *Synthetic Metals*, vol. 48, no. 1, pp. 91–97, 1992.
- [8] S. M. Sayyah, H.M. Abd El-Salam, and E. M. S. Azzam, "Surface activity of monomeric and polymeric (3-alkyloxy aniline) surfactants," *International Journal of Polymeric Materials*, vol. 54, no. 6, pp. 541–555, 2005.
- [9] S. M. Sayyah, A. A. Abd El-Khalek, A. A. Bahgat, and H. A. Abd El-Salam, "Kinetic studies of the chemical polymerization of substituted aniline in aqueous solutions and characterization of the polymer obtained Part 1. 3-Chloroaniline," *Polymer International*, vol. 50, no. 2, pp. 197–206, 2001.
- [10] S. M. Sayyah, A. A. Bahgat, and H. M. Abd El-Salam, "Kinetic studies of the aqueous oxidative polymerization of 3-hydroxyaniline and characterization of the polymer obtained," *International Journal of Polymeric Materials*, vol. 51, no. 3, pp. 291–314, 2002.
- [11] S. M. Sayyah and H. M. Abd El-Salam, "Aqueous oxidative polymerization of N-methyle aniline in acid medium and characterization of the obtained polymer," *International Journal of Polymeric Materials*, vol. 52, pp. 1087 – 1111, 2003.
- [12] S. M. Sayyah, A. A. Abd El-Khalek, A. A. Bahgat, and H. M. Abd El-Salam, "Kinetic studies of the polymerization of substituted aniline in aqueous solutions and characterization of the polymer obtained. Part 2. 3-methylaniline," *International Journal of Polymeric Materials*, vol. 49, no. 1, pp. 25–49, 2001.
- [13] S. M. Sayyah, H.M. Abd El-Salam, and A. A. Bahgat, "Aqueous oxidative polymerization of 3-methoxyaniline and characterization of its polymer," *International Journal of Polymeric Materials*, vol. 51, no. 10, pp. 915–938, 2002.
- [14] S. M. Sayyah, A. A. Bahgat, and H. M. Abd El-Salam, "Kinetic studies of the aqueous oxidative polymerization of 3-hydroxyaniline and characterization of the polymer obtained," *International Journal of Polymeric Materials*, vol. 51, no. 3, pp. 291–314, 2002.
- [15] S. M. Sayyah, A. A. Aboud, and S. M. Mohamed, "Chemical Polymerization Kinetics of Poly-O-Phenylenediamine and Characterization of the Obtained Polymer in Aqueous Hydrochloric Acid Solution Using  $K_2Cr_2O_7$  as Oxidizing Agent" *Hindawi Publishing Corporation International Journal of Polymer Science Volume 2014*.
- [16] S. M. Sayyah, Ahmed A. Aboud, Amgad. B. Khaliel and Salama. M. Mohamed, "Oxidative Chemical Polymerization of Ortho-Tolidine in Acid Medium Using  $K_2Cr_2O_7$  as Oxidizing Agent and Characterization of the Obtained Polymer" *International Journal of Advanced Research volume 2 (2014)*.
- [17] A. D. Becke. *J. Chem .phys.* 98,1993.5648-5682.
- [18] C. Lee. W. Yang and R.G. Parr, *Phys. B* 37, 1998,785-789.
- [19] Gaussian 09, Revision A. I. M. I.
- [20] P. Chowdhury and B. Saha, "Potassium dichromate initiated polymerization of aniline," *Indian Journal of Chemical Technology*, vol. 12, pp. 671–675, 2005.

- [21] S. M. Sayyah and H. Abd El Salam, "Oxidative chemical polymerization of some 3-alkyloxyaniline surfactants and characterization of the obtained polymers," *International Journal of Polymeric Materials and Polymeric Biomaterials*, vol. 55, no. 12, pp. 1075–1093, 2006.
- [22] Rahaman, M., Chaki, T.K., Khastgir, D., (2012). Consideration of interface polarization in the modeling of dielectric property for ethylene vinyl acetate (EVA)/polyaniline conductive composites prepared through in-situ Polymerization of aniline in EVA matrix. *s.l.: European Polymer Journal*, 48: 1241–1248.
- [23] Sohi, N., Rahaman, M., Khastgir, D., (2011). Dielectric property and Electromagnetic interference shielding effectiveness of ethylene vinyl acetate based conductive composites: effect of different type of carbon fillers. *Polym Compos.*, 32:1148–54.
- [24] Pant, H.C., Patra, M.K., Negi, S.C, Bhatia, A, Vadera, S.R, Kumar, N. (2006). Studies on conductivity and dielectric properties of polyaniline–zinc sulphide composites. *Bull Mater Sci .*, 29:379–384.
- [25] Dyre, J. C., (1988). "The random free energy barrier model for ac conduction in disordered solids". *J. Appl. Phys.*, 64(5) :2456.
- [26] A. K.Tomara., M.Suman., C.Rishi Pal, and K. Shyam., (2012). Structural and dielectric spectroscopic studies of polyaniline–poly (methylmethacrylate) composite films. *s.l.: Synthetic Metals*, 162: 820– 826.
- [27] Mardare, D., Rusu, G.I., and Optoelectron, J., (2004). Comparison of the dielectric properties for doped and undoped TiO<sub>2</sub> thin film. *Adv. Mater.*, 6(1): 333-336.
- [28] Paphanassiou. A., (2002). The power law dependence of the a.c. conductivity on frequency in amorphous solids. *J. Phys. D. Applied. Phys.* 35: 17.
- [29] Dey, A., De, S. and Sk, D. (2004). Characterization and dielectric properties of polyaniline–TiO<sub>2</sub> nanocomposites. *Nanotechnology*.15: 1277.
- [30] Elliott, S. (1987). a.c. conduction in amorphous chalcogenide and pnictide semiconductors *Adv. Phys.* 36: 135.